Jurnal Kejuruteraan 32(4) 2020: 637-644
https://doi.org/10.17576/jkukm-2020-32(4)-11

Effect of Heat Treatment on the Structural, Morphology and Electrochemical Performance of Perovskite $Ba_{0.5}Sr_{0.5}Co_{0.8}Fe_{0.2}O_{3-\delta}$-$Sm_{0.2}Ce_{0.8}O_{1.9}$ Carbonate Protective Coating for SOFC Metallic Interconnect

Tan Kang Huai, Hamimah Abd.Rahman* & Hariati Mohd Taib

[a]*Faculty of Mechanical and Manufacturing Engineering, Universiti Tun Hussein Onn Malaysia, 86400 Parit Raja, Batu Pahat, Johor, Malaysia*

**Corresponding author: hamimah@uthm.edu.my*

Received 17 July 2019, Received in revised form 07 November 2019
Accepted 16 December 2019, Available online 30 November 2020

ABSTRACT

A composite perovskite $Ba_{0.5}Sr_{0.5}Co_{0.8}Fe_{0.2}O_{3-\delta}$-$Sm_{0.2}Ce_{0.8}O_{1.9}$ carbonate (BSCF-SDCC) coating was investigated to enhance the performance of SUS 430 stainless steel as interconnect material for solid oxide fuel cells (SOFCs). BSCF-SDCC powder was successfully obtained by low-speed wet milling method from commercial BSCF, SDC, and binary carbonates. The developed BSCF-SDCC powder were heat-treated 600 °C for 90 min, and then characterized by X-ray diffraction (XRD) and field-emission scanning electron microscopy (FESEM) equipped with energy-dispersive spectroscopy (EDS). FESEM revealed better morphology of BSCF-SDCC powder with heat treatment. However, XRD analysis showed the destruction of BSCF phase in the BSCF-SDCC powder after heat treatment at 600 °C. Moreover, electrophoretic deposition (EPD) of BSCF-SDCC powder in an ethanol-added dispersing agent suspension was investigated under 10 volt 10 minutes by 10 g/l. The coated samples were then heat-treated at 600 °C. The coated samples were characterized by comparing between the samples with and without heat treatment based on XRD, SEM-EDS, and area specific resistance (ASR) analyses. XRD analysis indicated BSCF phases disappeared for the samples with heat treatment. The heat-treated sample performed better coating morphology and fewer pores. The samples underwent 500 hours of air oxidation at 600°C, and ASR was measured by DC 2-point method during in situ oxidation process. The coated sample with heat treatment at 600 °C exhibited excellent low area-specific resistance reading of below 0.1 Ωcm2, which is an essential requirement for interconnect materials. After 500 h of oxidation, the XRD patterns revealed stable phase and maintained good coating morphology.

Keywords: $Ba_{0.5}Sr_{0.5}Co_{0.8}Fe_{0.2}O_{3-\delta}$; electrophoretic deposition; interconnect; perovskite coating; solid oxide fuel cell

INTRODUCTION

Solid oxide fuel cells (SOFC) have attracted considerable attention owing to its quality efficiency, fuel flexibility, and environmentally friendliness (Pandet et al. 2019). An interconnect is a key component in the stack of planar SOFCs that separate hydrogen at anode and oxidant at cathode while simultaneously electrically connecting single cells to form a circuit. With lowering of SOFC operating temperature, stainless steel, such grade SUS430, Crofer 22 APU, and AISI 440, have been broadly applied as SOFC interconnect material due to machining availability, inexpensiveness, easy fabrication, and match thermal expansion with adjacent cells (Wei et al. 2007; Rufner et al. 2008). However, stainless steel with high oxidation resistance typically contains chromium (Cr), which volatizes at high temperature. Cr_2O_3 scale is formed and becomes thicker, which is a main key hindrance for electric conductivity (Bianco et al. 2019). In addition, the Cr_2O_3 scale vaporizes to become $Cr(OH)_2O_2$,which migrates and poisons the electrode. As a result, the performance of SOFC degrades obviously. Therefore, conductive protective coating is indispensable to achieve anti-oxidative ability of stainless steel, depress growth of the scale, and ensure electrical conductivity. Among coating techniques, electrophoretic deposition (EPD) has been considered due to its wide range of material availability, cost-effectiveness, and easy set-up (Amrollahi et al. 2016).

Spinel coating is widely used as protective layer on interconnects. $CuFe_2O_4$, $MnCO_2O_4$, and $CuMn_{1.8}O_4$ are effective in depressing Cr diffusion, generally denoting area specific resistance (ASR) of 0.0143 Ωcm^2, 0.05 Ωcm^2, and 0.0218 Ωcm^2, respectively, at intermediate to high temperature SOFC (800 °C to 1000 °C) (Hosseini et al. 2016; Talic et al. 2019; Sun et al. 2018). The readings from those spinel coatings are below 0.1 Ωcm^2, which is an essential requirement of ASR for interconnect application (Piccardo et al. 2007). Unfortunately, an investigation on interconnect coating for low-temperature SOFC (400 °C to 600 °C) has not been reported. Perovskite coating is generally a cathode material used for interconnect protective layer, such as LaSrCoFe (LSCF) and LaSrMn (LSM). They have been explored for interconnect coatings for intermediate to high-

temperature SOFC (Lee et al. 2010; Chen et al. 2017; Omar et al. 2018). BaSrCoFe (BSCF) is a cathode material that has never been studied as interconnect protective layer. BSCF is a good electronic conductor and can achieve the lowest area polarization resistance among perovskite materials in cathode application (Mosialek et al. 2016). BSCF also has less interaction and minimal reaction with volatized chromia scale from stainless steel interconnect (Jang et al. 2014)]. For low-temperature SOFC, an electrolyte samarium-doped ceria carbonate (SDCC), is embedded into perovskite cathode, such as LSCF-SDCC and SSCF-SDCC, which exhibit promising cathode characterization [Rahman et al. 2013; Mohammad et al. 2018; Muchtar et al. 2018. In the current study, SDCC is embedded into BSCF by milling technique. The developed BSCF-SDCC composite powder is deposited on stainless steel grade SUS 430. From past studies, BSCF was reported to have a suffocating unstable material compatibility at high-temperature oxygen environment (Ng et al. 2017). Hence, the effect of heat treatment on the developed BSCF-SDCC composite powder and deposited BSCF-SDCC on stainless steel interconnect is evaluated.

MATERIALS AND METHODS

PREPARATION OF BSCF-SDCC POWDER

Preparing commercial 80 wt% SDC (Sigma Aldrich) and 20 wt% binary carbonates (67 mol% $LiCO_3$ and 33 mol% $NaCO_3$) (Sigma Aldrich) by solid-state reaction. Then, SDC, $LiCO_3$, and $NaCO_3$ were mixed and milled at 150 rpm for 24 h. The obtained homogenous slurry SDCC was dried in an oven and heat-treated at 680 °C for 60 min. Subsequently, the developed 50 wt% SDCC was mixed with 50 wt% commercial $Ba_{0.5}Sr_{0.5}Co_{0.8}Fe_{0.2}O_{3-\delta}$ (BSCF) (Sigma Aldrich) and ball-milled (Fritsch Pulverissete 6, Germany) using zirconia ball and bowl as milling medium. The milling process was done in ethanol with 150 rpm for 2 h. The slurry BSCF-SDCC was dried in oven for 12 h. The BSCF-SDCC was heat-treated at 600 °C for 2 h. The developed BSCF-SDCC composite powders were designated as BSCF-SDCC (without heat treatment), 600 BSCF-SDCC (heat-treated at 600 °C), whereas coated samples were designated as SS coated BSCF-SDCC (without heat treatment) and 600 SS coated BSCF-SDCC (with heat treatment at 600 °C)

CHARACTERIZATION OF BSCF-SDCC POWDER

Field-emission scanning microscopy (FESEM, JEOL JSM 7600F, Japan) and X-ray diffraction (XRD, Bruker D8 Advance, Germany) with Cu Kα radiation (λ=0.15418) were used to identify the morphology and crystalline phase of BSCF-SDCC powder. The morphology was examined in the magnification scale of 100 nm. The diffraction patterns were collected by step scanning of 0.02° in the 2Θ range 20° to 90°.

ELECTROPHORETIC DEPOSITION (EPD) OF BSCF-SDCC PEROVSKITE COATING

Rectangular samples of 1 cm × 1.5 cm stainless steel were prepared from commercial stainless steel (SS) sheet grade SUS 430. The square stainless steels were ground with SiC sand paper to remove surface defects. Afterwards, the residue from grounding process was cleaned with acetone in ultrasonic bath for 10 min, followed by rinsing with deionized water. Cathodic electrophoretic deposition was performed in a 100 ml glass beaker cell. The counter electrode was stainless steel sheet (5 cm × 2 cm) bent in U-shape covering substrate by 1 cm distance. The EPD suspension was prepared in full ethanol with concentration 10 g/l BSCF-SDCC loading. Polydiallyldimethylammonium chloride (PDADMAC) as dispersing agent was dropped into the suspension by 10 µl for the loading. The suspension was prepared in pH 8, which was prior determined by zeta potential analysis (Malvern, UK) to be the most stable suspension pH. Then, the suspension was homogenized by electric sonicator for 5 min. EPD is a process where electric charge applied to conductive particle in a suspension. The charged particle deposits to the electrode of opposite charge (Katekar et al. 2019). The deposition process was done at 10 V for 10 minutes, which had been determined as optimal EPD coating parameters (Tan et al. 2018). The coated samples were heat treated at 600 °C.

CHARACTERIZATION OF BSCF-SDCC COATING

The crystalline phases of coated BSCF-SDCC with and without heat treatment were examined by XRD with same parameter as powder characterization. Meanwhile, the coating surface morphology and thickness (100 µm magnification scale) for both samples were observed via SEM (Hitachi, SU1510, Japan). Area specific resistance (ASR) was measured as a function of holding time and temperature in air by DC 2-point 4-probe method. Both samples were cut into 0.5 cm × 0.5 cm and then subjected to 500 h of oxidation at 600 °C. The ASR was taken every 48 h during oxidation. ASR was analyzed by Nova Autolab software version 1.11 and calculated using equation 1 below following Ohm's law.

$$ASR = \frac{1}{2}(R\,x\,A) \tag{1}$$

where A is coated surface area, R is resistance, and factor of 1/2 is used to show the role of one surface.

RESULTS AND DISCUSSION

POWDER CHARACTERIZATION

Figure 1 shows the morphology of the composites. BSCF-SDCC without heat treatment was more agglomerate, as shown in Figure 1(a). Milling process broke down particles

into larger surface area and higher surface energy which caused agglomeration by high attraction between particles (Hosokawa et al. 2018). Particles stick to one another, and their shapes were unclear. The particle shape was sharper for 600 BSCF-SDCC after heat treatment. Particle shape of BSCF-SDCC were appeared clearly because after milling process, heat treatment had been done on BSCF-SDCC. Heat treatment helped in growing the particle and refining the particle shape (Rahman et al. 2010). Elevated temperature confined small particles to grow and refine shape. Particles growth increase surface area and reduce surface energy. Thus, agglomeration was avoided.

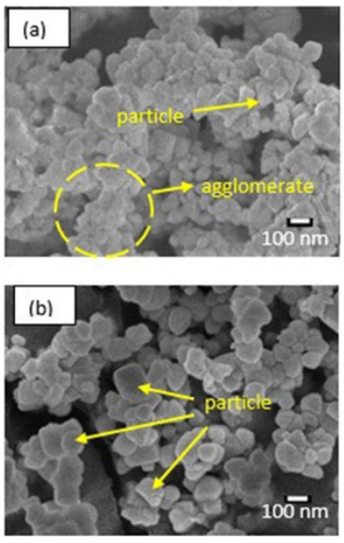

FIGURE 1. FESEM image of (a) BSCF-SDCC powder and (b) 600 BSCF-SDCC powder

For the assembling phase identification in Figure 2, the pure phases of BSCF (JCPDS No. 01-079-5253) and SDC phases (JCPDS No. 01-075-0158) were highly denoted in BSCF-SDCC composite powders. Milling process remained the denoting phases of SDC and BSCF after speed spinning. Carbonate was in amorphous phase as heat treatment had been conducted on SDCC as discussed. SDCC was heat-treated at 680 °C, at which binary carbonates melted and acted as shelter for SDC particles, thus avoiding the reduction of Ce^{4+} to Ce^{3+} that was essential for ionic conduction (Hoa et al. 2016). For 600 BSCF-SDCC, after 600 °C heat treatment, the SDC phase was distinct but there was insignificant BSCF phase detected owing to BSCF phase destruction by CO_2 at high temperature (Tan et al. 2018). Ba^{2+} evacuated from A site ions by CO_2 in high temperature environment, forming secondary phases, as shown indicated by 2 theta 23° and 52°, which had been detected as $BaCO_3$. For BSCF-SDCC without heat treatment, the peaks of SDC and BSCF phases were clear and vivid. There was also no secondary phases after milling process. Hence, the composite powder BSCF-SDCC without heat treatment was selected for EPD process as all complete phase confirmation, even though slight imperfection in morphology was observed.

Figures 3 and 4 display the morphology and coating thickness of SS coated BSCF-SDCC and 600 SS coated BSCF-SDCC on stainless steel SUS 430. Both samples possessed well particle deposition morphology. Figure 3 (a) and Figure 4 (a) show that the coating surface of 600 SS coated BSCF-SDCC appeared flat and compact. The coating thickness of 600 SS coated BSCF-SDCC was reduced from 128 µm to 95.2 µm after heat treatment because of shrinkage during heat treatment process. Heat treatment led to compact and dense coating because heat treatment assisted the healing of particle shape and reduce particle size. Dense and compact coating was very important as it could lessen diffusion of chromium to be volatized (Sun et al. 2019). As shown in Figure 5, distinct single phases of BSCF and SDC phases were detected after the BSCF-SDCC powder had been coated on stainless steel SUS430. After heat treatment, 600 SS coated BSCF-SDCC showed significant SDC phase. There were peaks of BSCF appearing in sample 600 SS coated BSCF-SDCC film unlike 600 BSCF-SDCC powders, indicating that BSCF phase was absent after heat treatment. Thus, when BSCF-SDCC was in thin film form, less CO_2 could diffuse into the smaller pores of SS coated 600 BSCF-SDCF. Moreover, Ba^{2+} ions retained its position stably in its cubic phase from CO_2 attack by compact and dense coating. Therefore, destruction of BSCF during heat treatment process was less promising in 600 SS coated BSCF-SDCC than powder form, only leading to minor formation of the secondary phase $BaCO_3$. The influence of this secondary phase towards ASR is discussed below.

Figure 6 shows the ASR parameters for SS coated BSCF-SDCC and 600 SS coated BSCF-SDCC. SS coated BSCF-SDCC without heat treatment showed increment of ASR from 0.0108 Ωcm^2 to 0.0169 Ωcm^2. Then, reading fluctuated over the 500 h oxidation. Thus, chromium diffusion and coating densification happened at the same time. Precipitation of Cr_2O_3 led to increased ASR and coating densification, which consequently led to the decrease in ASR (Zhao e. al, 2018). Accordingly, dense coating could achieve improved electric conductivity, which was the main reason that SS coated BSCF-SDCC did not achieve criteria of interconnect ASR which must below than 0.01 Ωcm^2 from beginning until the end.

However, the heat-treated sample, 600 SS coated BSCF-DCC, exhibited excellent ASR reading starting at 0.0669 Ωcm^2. The reading increased continuously from 0.067 Ωcm^2 achieving 0.0768 Ωcm^2 after 500 h of oxidation. The whole ASR was below the interconnect ASR requirement of 0.1 Ωcm^2 because of the dense and compact coating after heat treatment. Accordingly, the change in the ASR as a function of oxidation time is attributed to increment of thickness in the oxide scale (Magraso et al. 2015). Thus, the 600 SS coated BSCF-SDCC that was coated on the SUS430 could retard the oxidation of stainless-steel denoting insignificant formation of chromium scale. This ASR result was highly desirable for 600 SS coated BSCF-SDCC as achievement of

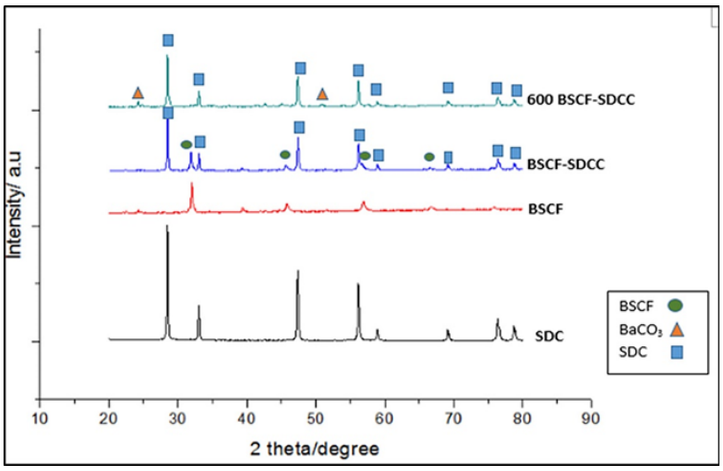

FIGURE 2. XRD spectra for BSCF-SDCC composite

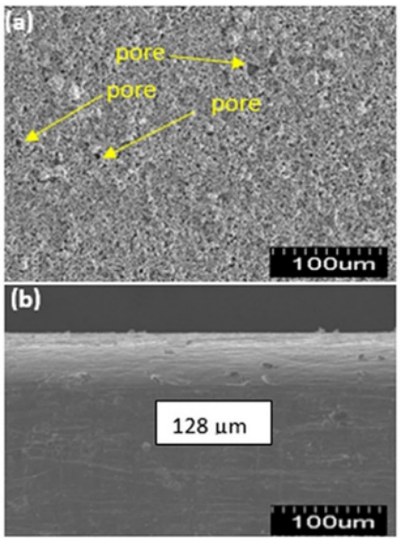

FIGURE 3. (a) Surface morphology and (b) coating thickness of SS coated BSCF-SDCC before heat treatment

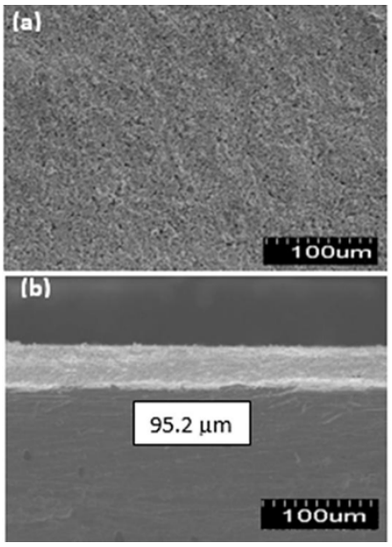

FIGURE 4. (a) Surface morphology and (b) coating thickness 600 SS coated BSCF-SDCC after heat treatment

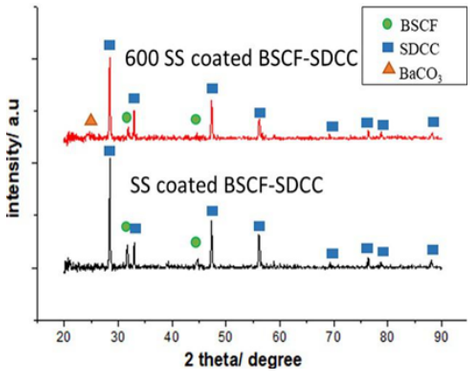

FIGURE 5. XRD profiles of coated samples

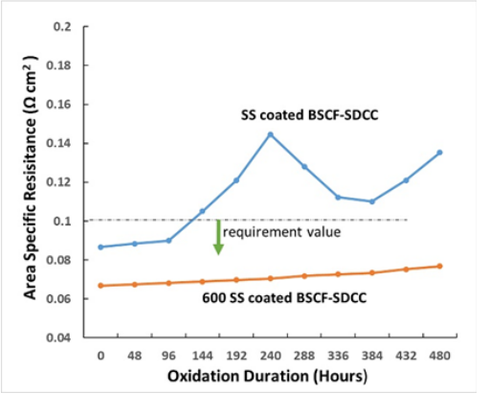

FIGURE 6. Area specific resistance (ASR) of coated samples along 500 hours oxidation

low ASR at low SOFC operating temperature. This agreed with previous study stating that heat treatment on perovskite material had significant influence on electrochemical performance (Baharuddin et al. 2016).

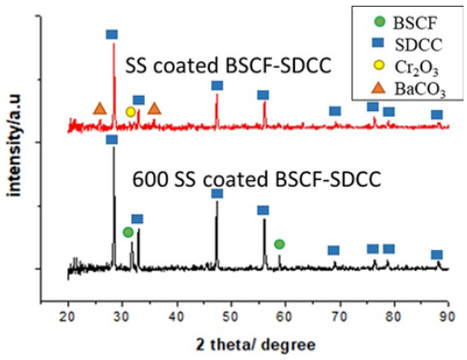

FIGURE 7. XRD profile of coated samples after 500 h oxidation

Figure 7 assemblies the changes of crystalline phases of SS coated BSCF-SDCC and 600 SS coated BSCF-SDCC after 500 h of oxidation at 600 °C. 600 BSCF-SDCC successfully maintained single purity phases of SDC and BSCF after long exposure to elevated temperature. However, destruction of BSCF phases was vividly observed in the sample without heat treatment, SS coated BSCF-SDCC. This was due to the reaction between BSCF and CO_2 in the air during the oxidation test hat leading to the formation of $BaCO_3$ secondary phases (Ng et al. 2017). After long exposure to oxidation, minor chromium oxide, Cr_2O_3 phase was also detected at 2 theta of 33° due to diffusion of chromium from the SUS430 (Zhang et al. 2018). Chromium diffusion through the pores was suggested at sample without heat treatment, SS coated BSCF-SDCC. Since SEM was conducted via black scattered method and dark spot is considered as pore as shown in Figure 8 (a). This was similar to the study that chromium diffused through the vacancy in the coating (Aznam et al. 2019). Heat treatment of thin film 600 SS coated BSCF-SDCC had led to robust bonding of perovskite crystalline structure and enhanced dense, uniform, and compact coating

Coating and morphology of coating SS coated BSCF-SDCC and 600 SS coated BSCF-SDCC were examined again after 500h of oxidation, as shown in Figures 8 and 9. The SS coated BSCF-SDCC coating surface was not flat and pores were more clearly seen. In monitoring the surface of 600 SS coated BSCF-SDCC, flat and dense morphology were still achieved after 500 h of oxidation. Furthermore, the thickness of SS coated BSCF-SDCC and 600 SS coated BSCF-SDCC was decreased compared to the previous thickness after heat treatment shown in Figures 3 and 4. Percentage of chromium diffusion was detected and determined through the difference between chromium atomic distribution between spectrum 1 and spectrum 2, as manifested in Figure 8 (b), 8(c), 9(b), 9(c), and Table 1.

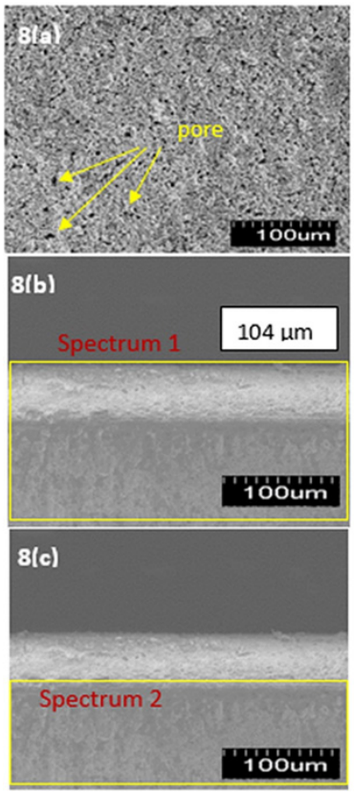

FIGURE 8. (a) Morphology of SS coated BSCF-SDCC. (b) EDS Spectrum 1, and (c) EDS Spectrum 2 after 500 h of oxidation

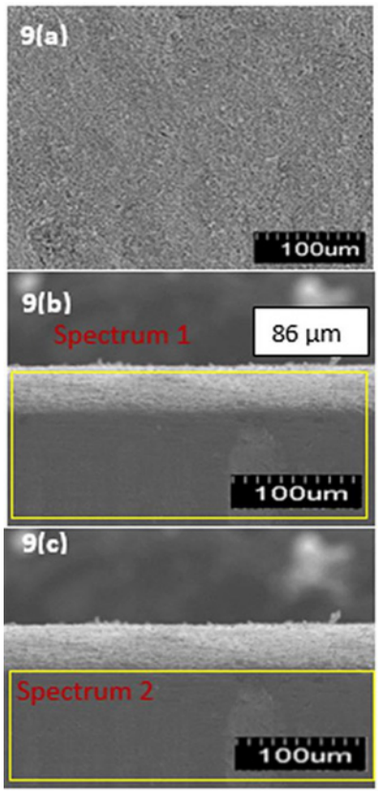

FIGURE 9. (a) Morphology of 600 SS coated BSCF-SDCC. (b) EDS Spectrum 1 and (c) EDS Spectrum 2 after 500 h oxidation

TABLE 1. Atomic distribution of coated samples after 500 hours oxidation

(a) Element	Atomic%	SS coated BSCF-SDCC
	Spectrum 1	Spectrum 2
C K	33.20	32.65
O K	36.16	35.39
Cr K	5.71	3.41
Fe K	19.37	27.39
Co K	1.49	0.47
Sr L	1.22	0.00
Ba L	1.16	0.47
Ce L	0.91	0.20
Sm L	0.78	0.02
Totals	100	100
(b) Element	Atomic%	600 SS coated BSCF-SDCC
	Spectrum 1	Spectrum 2
C K	31.50	29.17
O K	39.65	40.24
Cr K	4.34	4.22
Fe K	17.43	26.42
Co K	1.89	0.26
Sr L	1.62	0.08
Ba L	1.47	0.27
Ce L	1.11	0.19
Sm L	0.99	0.12
Totals	100	100

Sample SS coated BSCF-SDCC had higher diffusion of chromium from stainless steel to coating, which showed 2.3% difference between the EDS on spectrum 1 and spectrum 2, whereas sample 600 SS coated BSCF-SDCC only showed 0.12%. Thus, chromium had diffused more from stainless steel to the coating layer in SS coated BSCF-SDCC. This result was consistent with the XRD analysis showing the intensity of peak of Cr_2O_3 in SS coated BSCF-SDCC. The formation of Cr_2O_3 and reduction of coating thickness had proved diffusion and densification occurred in the midst of the oxidation process for SS coated BSCF-SDCC. Significantly low ASR of 600 SS coated BSCF-SDCC was evidenced by the dense uniform coating and retained BSCF and SDCC phases in low-temperature SOFC.

CONCLUSION

BSCF-SDCC has been developed by milling method. For powder preparation of BSCF-SDCC, heat treatment led to destruction of BSCF phase. Heat treatment on BSCF-SDCC powder was not favorable but suggested for BSCF-SDCC coating. Heat treatment at 600°C on BSCF-SDCC coating showed excellent coating morphology and remarkable ASR with 0.067- 0.076 Ωcm^2 for 600°C low-temperature SOFC. The findings proof that BSCF-SDCC coated layer exhibited suitable characteristics as interconnect perovskite coating for low-temperature SOFC. This paper is among the first to reporting on interconnect coating performance for low-temperature SOFCs.

ACKNOWLEDGEMENTS

The authors would like to thank the Ministry of Education Malaysia for supporting this research under Fundamental Research Grant Scheme No. FRGS/1/2016/TK05/UTHM/02/3 and partially sponsored by Universiti Tun Hussein Onn Malaysia under Postgraduate Research Grant Scheme (GPPS, U748).

DECLARATION OF COMPETING INTEREST

None.

REFERENCES

Amrollahi, P., Krasinski, J. S., Vaidyanathan, R., Tayebi, L., & Vashaee, D. 2016. Electrophoretic deposition (EPD): Fundamentals and applications from nano-to micro-scale structures. *Handbook of Nanoelectrochemistry: Electrochemical Synthesis Methods, Properties and Characterization Techniques*: 1-27.

Aznam, I., Wen, J. M. C., Muchtar, A., Baharuddin, N. A., Somalu, M. R., & Ghazali, M. J. 2019. Oxidation behaviour of

SUS430 ferritic stainless steel and effects of gaseous cr species volatilization on LSCF cathode surface in solid oxide fuel cell operating temperature. *Sains Malaysiana* 48(4): 861-869.

Baharuddin, N. A., Muchtar, A., Somalu, M. R., Sulong, A. B. & Abdullah, H. 2016. Effects of sintering temperature on the electrochemical performance of solid oxide fuel cell (SOFC) composite cathode LSCF-SDCC. *Sains Malaysiana* 45(3): 459-465.

Bianco, M., Tallgren, J., Hong, J. E., Yang, S., Himanen, O., Mikkola, J., & Steinberger-Wilckens, R. 2019. Ex-situ experimental benchmarking of solid oxide fuel cell metal interconnects. *Journal of Power Sources* 437: 226900.

Chen, J. W., Lin, K. Y., Yang, Y. C., & Yeh, S. T. 2017. Plasma-Sprayed LSM Protective Coating on Metallic Interconnect of SOFC. *Coatings* 7(12): 226.

Hanifi, A. R., Zahiri, B., Mitlin, D., Vincent, A. L., Etsell, T. H., & Sarkar, P. 2016. Effects of washing and calcination–milling on ionic release and surface properties of yttria stabilized zirconia. *Ceramics International* 42(6): 6755-6760.

Hoa, N. K., Abdul Rahman, H., & Rao Somalu, M. 2016. Preparation of nickel oxide-samarium-doped ceria carbonate composite anode powders by using high-energy ball milling for low-temperature solid oxide fuel cells. *Materials Science Forum* 840: 97-102.

Hosokawa, K., Yokoyama, T., Kondo, A., & Naito, M. 2018. Mechanical synthesis of composite oxide and its application for SOFC cathode. *In Nanoparticle Technology Handbook*: 505-510.

Hosseini, S. N., Karimzadeh, F., Enayati, M. H., & Sammes, N. M. 2016. Oxidation and electrical behavior of $CuFe_2O_4$ spinel coated Crofer 22 APU stainless steel for SOFC interconnect application. *Solid State Ionics* 289: 95-105.

Jiang, S. P., & Chen, X. 2014. Chromium deposition and poisoning of cathodes of solid oxide fuel cells–a review. *International Journal of Hydrogen Energy* 39(1): 505-531.

Khatekar, N. V., & Pawade, R. S. 2019. Analysis and modeling of surface characteristics in electrophoretic deposition–assisted internal polishing of AISI 304 steel. *The International Journal of Advanced Manufacturing Technology*: 1-12.

Lee, S., Chu, C. L., Tsai, M. J., & Lee, J. 2010. High temperature oxidation behavior of interconnect coated with LSCF and LSM for solid oxide fuel cell by screen printing. *Applied Surface Science*, 256(6): 1817-1824.

Magrasó, A., Falk-Windisch, H., Froitzheim, J., Svensson, J. E., & Haugsrud, R. 2015. *R*educed long term electrical resistance in Ce/Co-coated ferritic stainless steel for solid oxide fuel cell metallic interconnects. *International Journal of Hydrogen Energy* 40(27): 8579-8585.

Mohammad, S. F., Ahmad, S., Rahman, H. A., Muchtar, A., & Abdallah, K. S. 2018 Morphological and Physical Behaviour on the $Sm_{0.5}Sr_{0.5}CoO_{3-\delta}/Sm_{0.2}Ce_{0.8}O_{1.9}$ Incorporation with Binary Carbonate as Potential Cathode Materials for SOFC. *Key Engineering Materials* 791: 59-65.

Mosiałek, M., Kędra, A., Krzan, M., Bielańska, E., & Tatko, M. 2016. $Ba_{0.5}Sr_{0.5}Co_{0.8}Fe0.2O_{3-\delta}$–$La_{0.6}Sr_{0.4}Co_{0.8}Fe_{0.2}O_{3-\delta}$ composite cathode for solid oxide fuel cell. *Archives of Metallurgy and Materials* 61(3): 1483-1488.

Ng, K.H., Rahman, H.A., & Afandi, S. 2017. Effects of milling speed and calcination temperature on the phase stability of $Ba_{0.5}Sr_{0.5}Co_{0.8}Fe_{3-\delta.}$ In *Materials Science Forum* 888: 47-51.

Omar, N.I, Tan, K.H, Rahman, H.A. & Taib, H. 2018. Electrophoretic deposited LSCF-SDCC-Ag cathode coating on ferritic stainless steel interconnect for SOFC. *Journal of Physics*: Conference Series. 1082 (1): 012-028.

Pandey, A. 2019. Progress in Solid Oxide Fuel Cell (SOFC) Research. *The Journal of The Minerals, Metals & Materials Society* 71(1): 88-89.

Piccardo, P., Gannon, P., Chevalier, S., Viviani, M., Barbucci, A., Caboche, G., & Fontana, S. 2007. ASR evaluation of different kinds of coatings on a ferritic stainless steel as SOFC interconnects. *Surface and Coatings Technology* 202(4-7): 1221-1225.

Rahman, H. A., Muchtar, A., Muhamad, N., & Abdullah, H. 2010. $La_{1-x}Sr_xCo_{1-y}Fe_yO_{3-d}$ (LSCF) Composite as Durable Cathode Materials for Intermediate-Low Temperature Solid Oxide Fuel Cell: Research Review. *Jurnal Kejuruteraan* 22: 1-10.

Rahman, H. A., Muchtar, A., Muhamad, N., & Abdullah, H. 2013. $La_{0.6}Sr_{0.4}Co_{0.2}Fe_{0.8}O_{3-\delta}$–SDC carbonate composite cathodes for low-temperature solid oxide fuel cells. *Materials Chemistry and Physics* 141(2-3): 752-757.

Rufner, J., Gannon, P., White, P., Deibert, M., Teintze, S., Smith, R., & Chen, H. 2008. Oxidation behavior of stainless steel 430 and 441 at 800 C in single (air/air) and dual atmosphere (air/hydrogen) exposures. *International Journal of Hydrogen Energy* 33(4): 1392-1398.

Sun, Z., Gopalan, S., Pal, U. B., & Basu, S. N. 2019. Electrophoretically Deposited Copper Manganese Spinel Coatings for Prevention of Chromium Poisoning. *Energy Technology 2019: Carbon Dioxide Management and Other Technologies*: 265.

Sun, Z., Wang, R., Nikiforov, A. Y., Gopalan, S., Pal, U. B., & Basu, S. N. 2018. $CuMn_{1.8}O_4$ protective coatings on metallic interconnects for prevention of Cr-poisoning in solid oxide fuel cells. *Journal of Power Sources* 378: 125-133.

Talic, B. 2019. Investigation of electrophoretic deposition as a method for coating complex shaped steel parts in solid oxide cell stacks. *Surface and Coatings Technology*: 125093.

Tan, K. H., Rahman, H. A., Taib, H., Ahmad, S., Yusop, U. A., & Ibrahim, H. 2018. Influence of heat treatment and milling speed on phase stability of $Ba_{0.5}Sr_{0.5}Co_{0.8}Fe_{0.2}O_{3-\delta}$ composite cathode solid oxide fuel cell. *Key Engineering Materials.* 791: 66-73.

Tan, K.H., Rahman, H.A., and Taib, H. 2018. Electrophoretic Deposition of $Ba_{0.5}Sr_{0.5}Co_{0.8}Fe_{0.2}O_{3-\delta}$-SDC carbonate composite coating on solid oxide fuel cell interconnect. *Malaysian Journal of Microscopy* 14: 88-94.

Wei, P., Deng, X., Bateni, M. R. R., & Petric, A. 2007. Oxidation behavior and conductivity of UNS 430 stainless steel and Crofer 22 APU with spinel coatings. *ECS Transactions* 7(1): 2135-2143.

Zhang, X., You, P. F., Zhang, H. L., Yang, X. G., Luo, M. Q., & Zeng, C. 2108. Preparation and performances of CuCo spinel

coating on ferritic stainless steel for solid oxide fuel cell interconnect. *International Journal of Hydrogen Energy* 43(6): 3273-3279.

Zhao, Q., Geng, S., Chen, G., & Wang, F. 2018. Application of sputtered $NiFe_2$ alloy coating for SOFC interconnect steel. *Journal of Alloys and Compounds* 769: 120-129.